Mendeleev Communications

Mendeleev Commun., 2025, **35**, 379–382

Synthesis of diamond microcrystals with a unique diversity of NiN_x color centers by spontaneous crystallization using a nickel catalyst and europium oxide

Vladimir Yu. Osipov,*[a] Fedor M. Shakhov,[a] Andrei D. Trofimuk[a] and Kazuyuki Takai[b]

[a] *Ioffe Institute, 194021 St. Petersburg, Russian Federation. E-mail: osipov@mail.ioffe.ru*
[b] *Department of Chemical Science and Technology, Hosei University, Koganei, 184-8584 Tokyo, Japan*

DOI: 10.71267/mencom.7649

Synthetic diamonds grown at high pressure and high temperature by spontaneous crystallization using a nickel catalyst and europium oxide additive exhibit emission spectra caused by a large morphological diversity of luminescence centers. It was found that most emission lines are associated with complex impurity centers of the NiN_x composition (consisting of several nickel and nitrogen atoms) in a covalent diamond lattice. It was shown that the addition of europium oxide promotes an increase in the concentration of nickel Ni_s^- centers in the crystals.

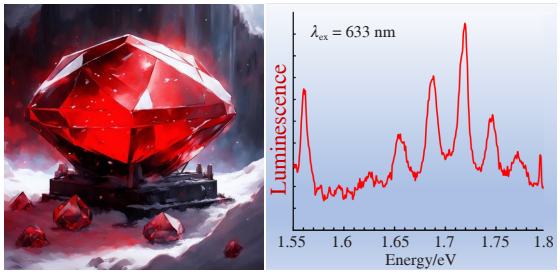

Keywords: synthetic diamond, high pressure and high temperature, nickel–nitrogen complexes, luminescence, electron spin resonance, solid state chemistry.

Synthesis of diamonds at high pressures and temperatures from graphite in the presence of a metal catalyst is a well-known method of growing diamonds for various applications in science and technology.[1–5] Under these conditions, the diamond phase can grow both with the use of specially introduced nucleation centers in the form of crystalline diamond seeds (the standard method) and without them (the method of the so-called spontaneous crystallization in a homogenized metal–carbon charge).[6] It should be noted that detonation nanodiamonds of 5 nm in size can also act as diamond growth seeds.[7,8] The catalysts are usually transition carbide-forming 3*d* metals with intermediate reactivity.[3] The use of nickel or nickel-containing alloys[9] as metal catalysts has been known for quite a long time and, as a rule, leads to the formation of nickel-based optical centers in the growing diamond matrix.[10,11] Many of such centers have been successfully identified previously.[11–15] Nickel-based centers can be used as emission centers in the spectral range above 800 nm and have various applications in nanophotonics.[16–18]

The role of the metal catalyst in the diamond synthesis process is quite complex, but it is generally accepted that during synthesis at temperatures above 1300 °C and pressures of about 5 GPa, the following processes occur.[6,19] Nickel melts and carbon gradually dissolves in the nickel melt. Carbon dissolved in a small portion of the nickel melt undergoes mass transfer in it, and when this portion leaves the melt zone, micron-sized diamond crystallites are formed.

Due to the presence of air in the high-pressure chamber, the grown diamond crystals also contain nitrogen in the form of isolated impurities, dimers or even aggregates of atoms. If a nitrogen getter is not used in the synthesis process, the nitrogen content in the grown crystals is *a priori* high (more than 350 ppm). In general, diamond microcrystals synthesized using a nickel catalyst without a nitrogen getter should contain polyatomic complexes (centers) of the NiN_x type, in which nickel atoms are surrounded by a different number of nitrogen atoms and carbon vacancies.[11,20] The appearance of polyatomic complexes based on nickel and nitrogen is also facilitated by annealing the synthesized crystals at temperatures above 1600 °C.[20] Given the potential diversity of atomic forms built from nitrogen, nickel and vacancies in different quantities, one should also expect a diversity of luminescent centers in such crystals. The main objective of this work was to search for new luminescent centers of the NiN_x type with unique spectral signatures in diamonds synthesized with a nickel catalyst. To implement this task, we chose the technique of rapid (up to 90 s) diamond synthesis by spontaneous crystallization from a mixture of microcrystalline graphite and powdered nickel. To test the possibility of doping the grown crystals with europium ions,[21] the effect of adding europium(III) oxide to the reaction mixture was additionally studied by analogy with the published work.[22]

The charge status of nickel impurities in the diamond lattice and its identification by electron paramagnetic resonance (EPR) have been discussed previously in the literature, including our recent study.[23,24] The spin of nickel impurity in the neutral substitutional state (Ni_s^0) is two, and upon capture of one electron (Ni_s^-) it becomes 3/2 with the electronic configuration $3d^7$.[23,25]

In this work, we analyze the EPR spectra and fluorescence spectra of microcrystalline diamond synthesized using a high-pressure chamber (P = 5.0–5.5 GPa, pressing at a high temperature close to 1650 °C) and nickel as a catalyst metal. Europium oxide (Eu_2O_3) was additionally introduced into the carbon–nickel charge subjected to pressing as a modifying/inhibiting additive in an amount of 5 wt% (see Online Supplementary Materials) to obtain microcrystalline diamond powder D1-bis.[†] The synthesis time at the maximum temperature was about 90 s. Microcrystalline

[†] The europium content of D1-bis diamonds is about 7 ppm, based on X-ray fluorescence analysis (see Online Supplementary Materials).

diamond powder synthesized without europium oxide was also obtained as a reference sample D1. In both cases, a nitrogen getter such as aluminum was not added to the batch in order to obtain the highest possible nitrogen content in the grown diamond crystals. Some details of the synthesis of microdiamonds using a nickel catalyst have been published previously.[26,27]

Scanning electron microscopy images of both types of synthesized diamonds are shown in Figure S1 (see Online Supplementary Materials). The average size of microcrystals in both cases is about 80 μm. The grown microcrystals D1 and D1-bis have an arbitrary shape, far from regular faceting, although a small number of almost perfect crystals of octahedral and other shapes are found among them. This is due to the short synthesis time, which does not allow for the formation of defect-free crystals with an octahedral habit.

Figure 1 shows the EPR spectra[‡] of samples D1 and D1-bis recorded at 90 K. Both spectra contain triplet EPR signals from paramagnetic nitrogen with spin $S = 1/2$ (the so-called P1 signal[28] with the centerline g-factor of 2.0024) and singlet EPR signals from the nickel defect Ni_s^- with spin $S = 3/2$ in the electronic configuration $3d^7$ (the so-called W8 signal[23,25,29] with the g-factor of 2.0319), located in the recording range at ~319 mT. All individual lines forming the EPR spectrum of each sample are quite broad. Specific features associated with orientational averaging of the paramagnetic nitrogen signal in the powder, which are usually observed in microcrystalline diamonds with a nitrogen content below 150 ppm, are not even visible. This is due to the strong broadening of the EPR lines of all paramagnetic agents in the system due to the presence of a prevalent broadening paramagnetic agent, *i.e.*, substitutional nitrogen. To correctly separate the EPR spectrum of each sample into individual components, each spectrum was integrated [Figure S2(*a*),(*b*)] and the resulting integrated spectra were decomposed into contours from substitutional nitrogen (three lines at ~320.56, ~323.7 and ~326.9 mT), nickel Ni_s^- (at ~319.1 mT) and one broad contour (at ~323.7 mT) from an unknown paramagnetic agent. This broad signal at ~323.7 mT, lying under the central signal of the nitrogen triplet ($g = 2.0024$), can be associated with centers of non-nitrogen origin, such as negatively charged vacancies with spin $S = 3/2$ or compact paramagnetic clusters based on several neighboring nitrogen atoms.[30,31] For sample D1-bis, the signal intensity from the substitution nickel, normalized to the integral intensity of the triplet signal P1, is approximately 1.5 times greater than for sample D1 (0.197 *vs.* 0.121).

The concentrations of substitutional nitrogen Ni_s^0 and substitutional nickel in the Ni_s^- state in microcrystalline powders, estimated using the method described earlier,[24] are 404 and 9.8 ppm in sample D1 and 380 and 15 ppm in sample D1-bis, respectively. It is evident that the concentration of Ni_s^- centers in sample D1-bis is approximately 1.5 times greater than in sample D1, while the concentration of substitutional nitrogen is only 1.06 times lower. This makes the D1-bis microcrystals more interesting from the point of view of the presence of nickel-containing optical centers.[§]

Luminescence spectra[¶] of individual particles of D1-bis microcrystals recorded at different excitation wavelengths are shown in Figures 2 and S3 for different groups of identified particles 1, 2, 3, 5 and 6 defined below. It is evident that the luminescence spectra from different particles are quite diverse and the spectra contain signatures from NV^-,[††] NiN_x emission centers, nitrogen-free nickel-based centers and other lattice defects.

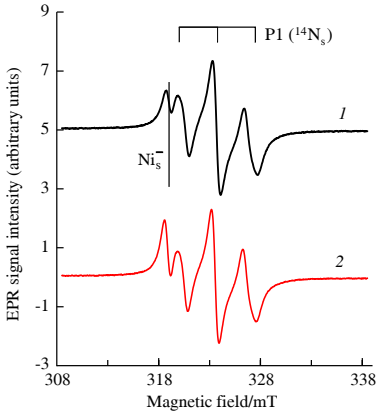

Figure 1 EPR spectra of (*1*) sample D1 and (*2*) sample D1-bis recorded at 90 K. The peak intensities of the central components of both signals at 323.6 mT ($g = 2.0024$) are normalized to the same value. The triplet structure of the P1 signal is due to the hyperfine splitting from the ^{14}N nuclear spins.

Thus, upon optical excitation at wavelengths of 532 and 633 nm, the following particles can be detected: particles with emission spectra only from NV^- centers (group 1); particles with emission lines at 602 and 618 nm from NiN_x centers and other characteristic low-intensity lines in the spectral range of 640–750 nm (group 2); particles with a characteristic unique pattern of six emission lines at 700.0, 710.3, 721.6, 735.2, 749.1 and 763.8 nm from NiN_x centers and a separate emission line at 794.7 nm from NE8[‡‡,32] centers (group 3); particles with a zero-phonon line (ZPL) at 746.9 nm, vibrational replicas at 774.9 and 805.1 nm (1.66 eV line system) in the spectral pattern and emission lines at 794.8 (ZPL), 812.5 and 830.9 nm (vibrational replicas in the 1.56 eV line system) from NiN_x centers (group 4); as well as particles with a single high-intensity emission line at 883 nm from Ni_s^+ and/or the so-called NE4[§§,32] centers (group 5). The luminescence spectra of group 4 particles have been studied recently[33] and are not considered here. A small fraction of particles (group 6) exhibit emission spectra from NV^- centers together with characteristic emission lines of the Eu^{3+} ion (see Figure S3). In this case, for the precise identification of the spectral lines of the Eu^{3+} ion (intracenter $4f$ $^5D_0 \rightarrow {}^7F_{0,1,2,4}$ transitions) in the spectra of D1-bis particles, we used the emission spectrum of europium oxide microparticles recorded at the same excitation wavelength of 532 nm (see Figure S3). It can be assumed that in the last group of particles, the luminescence of Eu^{3+} ions occurs as a result of the incorporation of fragments of the crystal lattice of the europium oxide used (no larger than 500–800 nm in size) or even isolated Eu^{3+} ions into the growing diamond crystallites during the synthesis.

The above-mentioned sextet of spectral lines contains a zero-phonon emission line at 721.6 nm and three intense lines at 735.2, 749.1 and 763.8 nm, associated with different energies of localized vibrational modes[¶¶,34] of the nickel atom in the complex, differing by 32 meV [Figure 2(*a*)]. The other two lines of the sextet at 700.0 and 710.3 nm are apparently due to other zero-phonon radiative transitions in the observed fluorescent complex, occurring only in

[‡] EPR spectra were recorded at a microwave frequency of 9.071 GHz using an X-band EPR spectrometer. The parameters for recording the EPR data and the methods for processing the integral EPR spectra were described by us earlier.[24]

[§] The nickel content in both samples, according to X-ray fluorescence analysis, is in the range of 520–1030 ppm, which indicates the predominance of other forms of nickel in these crystals, for example, nanosized Ni clusters.

[¶] Luminescence spectra were recorded using excitation wavelengths of 532 and 633 nm.

[††] Here the symbol V means a vacancy in the diamond lattice.

[‡‡] NE8 denotes a polyatomic complex consisting of one nickel atom, two semi-vacancies and four nitrogen atoms (N_2VNiVN_2) in the diamond lattice according to the nomenclature of nickel centers in diamond.

[§§] NE4 is the label assigned to a lattice defect representing a single nickel atom in an octahedral double semi-vacancy position $(VNiV)^-$.

[¶¶] A similar situation occurs for the emission lines of the tungsten complex in diamond.[34]

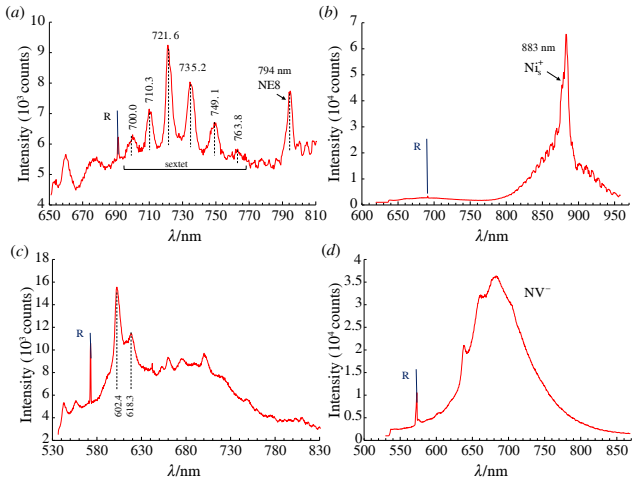

Figure 2 Luminescence spectra of individual D1-bis microcrystals assigned to particles of (*a*) group 3 (emission from NiN_x complexes and NE8 centers), (*b*) group 5 (emission from Ni_s^+ centers), (*c*) group 2 (emission from 602.4 and 618.3 nm fluorescence centers) and (*d*) group 1 (emission from NV^- centers). The spectra were recorded at 293 K using excitation wavelengths of (*a*),(*b*) 633 and (*c*),(*d*) 532 nm.

the group 3 particles. The broad spectral lines of this group of lines (ZPL at 721.6 nm) indicate that the heteroatoms forming this previously unstudied optical center are in carbon-substituting positions in the crystal with strong electron–phonon (lattice) interaction. The observation of a unique spectral pattern in the range of 695–770 nm with a characteristic distribution of the intensities of the spectral components has not been previously reported in the literature. In our study, such a spectral pattern is observed on a variety of synthesized diamond particles, and the characteristic intensity ratio of all six spectral components is preserved for all particles of group 3. It can be concluded that the fluorescent complex with such a spectral pattern consists of several major impurity atoms of nitrogen and nickel, including lattice vacancies, and, possibly, minor impurity atoms. Copper may also be among them (Table S1, see Online Supplementary Materials). This element uncontrollably enters the synthesized product during the synthesis from materials contained in the high-pressure cell.

All the main fluorescent spectral bands and lines noted in this study, except for the sextet lines in the 695–770 nm range, are well known and identified in the literature.[11,12,35] Among them are the fluorescence spectrum of NV^- centers [Figure 2(*d*)] and the intense lines at 794.7 and 883 nm from NE8 and Ni_s^+ centers, respectively [Figure 2(*a*),(*b*)].[30,36] In addition, for example, the emission lines at 602 and 618 nm, which constitute the unique spectral pattern of group 2 particles in the 590–640 nm range [Figure 2(*c*)], have been previously observed in nickel-enriched synthetic diamonds.[37] The emission lines of $^5D_0 \rightarrow {}^7F_2$ transitions in Eu^{3+} at 615.5 and 621.2 nm observed in Figure S3, together with other low-intensity bands at ~594 nm ($^5D_0 \rightarrow {}^7F_1$) and ~707 nm ($^5D_0 \rightarrow {}^7F_4$), are in good agreement with the luminescence spectrum of Eu_2O_3 particles.[38] However, the intensity of Eu^{3+} luminescence is at least ~30 times lower than the emission intensity of NV^- centers in the same group 6 of D1-bis particles.

It should be noted that the luminescence spectra of D1 microcrystals synthesized without the addition of europium(III) oxide also contained characteristic sextets of emission lines in the range of 695–770 nm, as well as emission bands from NV^- centers, respectively and bands at 794.7 and 883 nm. However, the study of luminescence in sample D1 did not reveal such a wide variety of accompanying luminescence centers in D1 microcrystals as was the case with sample D1-bis, including emission lines at 615.5 and 621.2 nm from Eu^{3+} ions. This indicates that the addition of europium oxide to the graphite–nickel charge is the cornerstone of the technique for producing diamond particles with different compositions of impurity polyatomic complexes and with a wide variety of characteristic spectral patterns for individual particles.

The method of synthesizing diamond particles with a nickel catalyst using the spontaneous crystallization mechanism and the addition of europium oxide makes it possible to obtain so-called 'low-grade' microcrystals with morphologically diverse (on an atomic scale) luminescent centers based on heteroatomic complexes NiN_x, NV^- and others.

Addition of europium oxide in an amount of up to 5 wt% to the metal–graphite charge made it possible to synthesize diamond microcrystals containing impurity nitrogen and nickel atoms in carbon-substituting positions in an amount of 380 and 15 ppm, respectively. At the same time, the introduction of europium oxide additive contributed to an almost one and a half-fold increase in the concentration of isolated negatively charged nickel atoms (Ni_s^-) in the crystals compared to the case without its use. At least six types of different diamond particles with specific spectral signatures of luminescence centers were found in the synthesized material. Among them are NiN_x, NV^-, Ni_s^+, nickel NE4 (883 nm) centers and others. One group of such particles exhibits a unique, previously unknown, very rich in detail spectral pattern, consisting of at least six lines of the same width in the range of 695–770 nm. These microcrystals could be used to develop nanophotonic devices and sensors that exploit the properties of individual particles with unique luminescent signatures.

This work was carried out within the framework of the Ioffe Institute project FFUG-2024-0019.

Online Supplementary Materials

Supplementary data associated with this paper can be found in the online version at doi: 10.71267/mencom.7649.

References

1 H. P. Bovenkerk, F. P. Bundy, H. T. Hall, H. M. Strong and R. H. Wentorf, Jr., *Nature*, 1959, **184**, 1094; https://doi.org/10.1038/1841094a0.
2 M. Stishov, *Phys.-Usp.*, 2019, **62**, 704; https://doi.org/10.3367/UFNe.2019.03.038545.
3 C.-M. Sung and M.-F. Tai, *Int. J. Refract. Met. Hard Mater.*, 1997, **15**, 237; https://doi.org/10.1016/s0263-4368(97)00003-6.
4 A. F. Khokhryakov, Y. M. Borzdov and I. N. Kupriyanov, *J. Cryst. Growth*, 2020, **531**, 125358; https://doi.org/10.1016/j.jcrysgro.2019.125358.
5 H. Kanda, M. Akaishi and S. Yamaoka, *Appl. Phys. Lett.*, 1994, **65**, 784; https://doi.org/10.1063/1.112230.
6 N. D. Zhigadlo, *J. Cryst. Growth*, 2014, **395**, 1; https://doi.org/10.1016/j.jcrysgro.2014.03.002.
7 N. A. Feoktistov, V. I. Sakharov, I. T. Serenkov, V. A. Tolmachev, I. V. Korkin, A. E. Aleksenskii, A. Ya. Vul' and V. G. Golubev, *Tech. Phys.*, 2011, **56**, 718; https://doi.org/10.1134/S1063784211050112.
8 M. G. Chernysheva, A. G. Popov, M. G. Dzianisik, A. V. Egorov, T. B. Egorova, A. V. Gopin, A. A. Mitrofanov and G. A. Badun, *Mendeleev Commun.*, 2023, **33**, 228; https://doi.org/10.1016/j.mencom.2023.02.025.
9 Y. N. Palyanov, A. F. Khokhryakov, Y. M. Borzdov and I. N. Kupriyanov, *Cryst. Growth Des.*, 2013, **13**, 5411; https://doi.org/10.1021/cg4013476.
10 H. Kanda and K. Watanabe, *Diamond Relat. Mater.*, 1999, **8**, 1463; https://doi.org/10.1016/S0925-9635(99)00070-9.
11 A. Yelisseyev and H. Kanda, *New Diamond Front. Carbon Technol.*, 2007, **17**, 127; https://www.mendeley.com/catalogue/9402f7d2-58c2-3bd1-9f9a-2b861dc6af17/.
12 A. M. Zaitsev, *Optical Properties of Diamond: A Data Handbook*, Springer, Berlin, 2001; https://doi.org/10.1007/978-3-662-04548-0.
13 V. Nadolinny and A. Yelisseyev, *Diamond Relat. Mater.*, 1994, **3**, 1196; https://doi.org/10.1016/0925-9635(94)90168-6.
14 L. Chen, W. Shen, C. Fang, Y. Zhang, P. Mu, G. Zhou, Q. Wang, Z. Zhang and X. Jia, *Cryst. Growth Des.*, 2020, **20**, 3257; https://doi.org/10.1021/acs.cgd.0c00080.
15 A. T. Collins, *Diamond Relat. Mater.*, 2000, **9**, 417; https://doi.org/10.1016/S0925-9635(99)00314-3.
16 I. Aharonovich and E. Neu, *Adv. Opt. Mater.*, 2014, **2**, 911; https://doi.org/10.1002/adom.201400189.

17 T. Gaebel, I. Popa, A. Gruber, M. Domhan, F. Jelezko and J. Wrachtrup, *New J. Phys.*, 2004, **6**, 98; https://doi.org/10.1088/1367-2630/6/1/098.
18 N. S. Kurochkin, V. V. Sychev, A. V. Gritsienko and D. Bi, *Phys. Status Solidi RRL*, 2024, **18**, 2300277; https://doi.org/10.1002/pssr.202300277.
19 S. Ferro, *J. Mater. Chem.*, 2002, **12**, 2843; https://doi.org/10.1039/B204143J.
20 R. N. Pereira, A. J. Neves, W. Gehlhoff, N. A. Sobolev, L. Rino and H. Kanda, *Diamond Relat. Mater.*, 2002, **11**, 623; https://doi.org/10.1016/S0925-9635(01)00578-7.
21 D. E. P. Vanpoucke, S. S. Nicley, J. Raymakers, W. Maes and K. Haenen, *Diamond Relat. Mater.*, 2019, **94**, 233; https://doi.org/10.1016/j.diamond.2019.02.024.
22 Y. N. Palyanov, Y. M. Borzdov, A. F. Khokhryakov and I. N. Kupriyanov, *Crystals*, 2019, **9**, 300; https://doi.org/10.3390/cryst9060300.
23 J. Isoya, H. Kanda and Y. Uchida, *Phys. Rev. B: Condens. Matter Mater. Phys.*, 1990, **42**, 9843; https://doi.org/10.1103/PhysRevB.42.9843.
24 V. Yu. Osipov, F. M. Shakhov, N. M. Romanov and K. Takai, *Mendeleev Commun.*, 2022, **32**, 645; https://doi.org/10.1016/j.mencom.2022.09.026.
25 J. Isoya, H. Kanda, J. R. Norris, J. Tang and M. K. Bowman, *Phys. Rev. B: Condens. Matter Mater. Phys.*, 1990, **41**, 3905; https://doi.org/10.1103/PhysRevB.41.3905.
26 F. M. Shakhov, A. M. Abyzov, S. V. Kidalov, A. A. Krasilin, E. Lähderanta, V. T. Lebedev, D. V. Shamshur and K. Takai, *J. Phys. Chem. Solids*, 2017, **103**, 224; https://doi.org/10.1016/j.jpcs.2016.11.020.
27 F. M. Shakhov, V. Yu. Osipov, A. A. Krasilin, K. Iizuka and R. Oshima, *J. Solid State Chem.*, 2022, **307**, 122804; https://doi.org/10.1016/j.jssc.2021.122804.
28 W. V. Smith, P. P. Sorokin, I. L. Gelles and G. J. Lasher, *Phys. Rev.*, 1959, **115**, 1546; https://doi.org/10.1103/PhysRev.115.1546.
29 A. T. Collins, H. Kanda, J. Isoya, C. A. J. Ammerlaan and J. A. van Wyk, *Diamond Relat. Mater.*, 1998, **7**, 333; https://doi.org/10.1016/S0925-9635(97)00270-7.
30 O. A. Shenderova, A. I. Shames, N. A. Nunn, M. D. Torelli, I. Vlasov and A. Zaitsev, *J. Vac. Sci. Technol., B: Nanotechnol. Microelectron.: Mater., Process., Meas., Phenom.*, 2019, **37**, 030802; https://doi.org/10.1116/1.5089898.
31 V. Yu. Osipov, F. M. Shakhov, N. N. Efimov, V. V. Minin, S. V. Kidalov and A. Ya. Vul', *Phys. Solid State*, 2017, **59**, 1146; https://doi.org/10.1134/S1063783417060191.
32 G. Thiering, E. Londero and A. Gali, *Nanoscale*, 2014, **6**, 12018; https://doi.org/10.1039/c4nr03112a.
33 I. E. Kaliya, V. Yu. Osipov, F. M. Shakhov, K. Takai, K. V. Bogdanov and A. V. Baranov, *Carbon*, 2024, **219**, 118839; https://doi.org/10.1016/j.carbon.2024.118839.
34 K. V. Bogdanov, I. E. Kaliya, M. A. Baranov, S. A. Grudinkin, N. A. Feoktistov, V. G. Golubev, V. Yu. Davydov, A. N. Smirnov and A. V. Baranov, *Materials*, 2022, **15**, 8510; https://doi.org/10.3390/ma15238510.
35 M. N. R. Ashfold, J. P. Goss, B. L. Green, P. W. May, M. E. Newton and C. V. Peaker, *Chem. Rev.*, 2020, **120**, 5745; https://doi.org/10.1021/acs.chemrev.9b00518.
36 A. I. Shames, A. Dalis, A. D. Greentree, B. C. Gibson, H. Abe, T. Ohshima, O. Shenderova, A. Zaitsev and P. Reineck, *Adv. Opt. Mater.*, 2020, **8**, 2001047; https://doi.org/10.1002/adom.202001047.
37 X. Miao, G. Liu, H. Ma, Z. Zhang, L. Zhou and X. Jia, *CrystEngComm*, 2021, **23**, 8110; https://doi.org/10.1039/D1CE00806D.
38 J. Lai, T. Wang, H. Zhang, L. Ye, C. Yan and W. Gu, *J. Lumin.*, 2019, **214**, 116534; https://doi.org/10.1016/j.jlumin.2019.116534.

Received: 14th October 2024; Com. 24/7649